RL-TR-95-6
Final Technical Report
January 1995

HIGH SPEED RANDOM ACCESS, FOURIER TRANSFORM HOLOGRAPHIC ASSOCIATIVE AND HIGH DENSITY TWO-PHOTON THREE-DIMENSIONAL OPTICAL MEMORIES BASED ON BACTERIORHODOPSIN

Syracuse University

Dr. Robert R. Birge

APPROVED FOR PUBLIC RELEASE; DISTRIBUTION UNLIMITED.

Rome Laboratory
Air Force Materiel Command
Griffiss Air Force Base, New York

This report has been reviewed by the Rome Laboratory Public Affairs Office (PA) and is releasable to the National Technical Information Service (NTIS). At NTIS it will be releasable to the general public, including foreign nations.

RL-TR-95-6 has been reviewed and is approved for publication.

APPROVED: Bernard J Clarke

BERNARD J. CLARKE, Captain, USAF
Project Engineer

FOR THE COMMANDER:

JOSEPH CAMERA
Acting Technical Director
Intelligence & Reconnaisance Directorate

If your address has changed or if you wish to be removed from the Rome Laboratory mailing list, or if the addressee is no longer employed by your organization, please notify RL (IRAP) Griffiss AFB NY 13441. This will assist us in maintaining a current mailing list.

Do not return copies of this report unless contractual obligations or notices on a specific document require that it be returned.

REPORT DOCUMENTATION PAGE

Form Approved
OMB No. 0704-0188

1. AGENCY USE ONLY (Leave Blank)	2. REPORT DATE	3. REPORT TYPE AND DATES COVERED
	January 1995	Final ----

4. TITLE AND SUBTITLE
HIGH SPEED RANDOM ACCESS, FOURIER TRANSFORM HOLOGRAPHIC ASSOCIATIVE AND HIGH DENSITY TWO-PHOTON (see reverse)

5. FUNDING NUMBERS
C - F30602-91-C-0084
PE - 62702F
PR - 4594
TA - 15
WU - H1

6. AUTHOR(S)
Dr. Robert R. Birge

7. PERFORMING ORGANIZATION NAME(S) AND ADDRESS(ES)
Syracuse University
Center for Molecular Electronics
Syracuse NY 13244-4100

8. PERFORMING ORGANIZATION REPORT NUMBER
N/A

9. SPONSORING/MONITORING AGENCY NAME(S) AND ADDRESS(ES)
Rome Laboratory (IRAP)
32 Hangar Rd
Griffiss AFB NY 13441-4114

10. SPONSORING/MONITORING AGENCY REPORT NUMBER
RL-TR-95-6

11. SUPPLEMENTARY NOTES
Rome Laboratory Project Engineer: Bernard J. Clarke, Captain, USAF/IRAP/ (315) 330-4581

12a. DISTRIBUTION/AVAILABILITY STATEMENT
Approved for public release; distribution unlimited.

12b. DISTRIBUTION CODE

13. ABSTRACT (Maximum 200 words)

The goals of this research and development program were to optimize bacteriorhodopsin based photochromic and photorefractive materials for use in optical memories. Two spatial light modulators (SLMs) based on bacteriorhodopsin were developed, one that could be controlled via applied voltage and the other controlled by light. The former performed below target specification, whereas the latter achieved diffraction efficiencies two-fold above target. Preliminary results on the three-dimensional data cube were sufficiently exciting to adjust the first year statement of work to also include the optimization of the bacteriorhodopsin data cube.

14. SUBJECT TERMS
3-D optical memories, Organic memories, Bacteriorhodopsin, Mass data storage

15. NUMBER OF PAGES
40

16. PRICE CODE

17. SECURITY CLASSIFICATION OF REPORT	18. SECURITY CLASSIFICATION OF THIS PAGE	19. SECURITY CLASSIFICATION OF ABSTRACT	20. LIMITATION OF ABSTRACT
UNCLASSIFIED	UNCLASSIFIED	UNCLASSIFIED	UL

4. (Cont'd)

THREE-DIMENSIONAL OPTICAL MEMORIES BASED ON BACTERIORHODOPSIN

Table of Contents

1. Abstract. Two-photon three-dimensional optical addressing architectures offer significant promise for the development of a new generation of ultra-high density random access memories. These memories read and write information by using two orthogonal laser beams to address an irradiated volume (1 - 50 μm^3) within a much larger volume of a nonlinear photochromic material. Because the probability that a molecule will absorb two-photons is proportional to the square of the intensity, photochemical activation is limited to a first approximation to regions only within the irradiated volume. (Methods to correct for photochemistry outside the irradiated volume are described below.) The three dimensional addressing capability derives from the ability to adjust the location of the irradiated volume in three dimensions. Two dimensional optical memories have a storage capacity that is limited to ~$1/\lambda^2$, where λ is the wavelength, which yields approximately 10^8 bits/cm^2. In contrast, three-dimensional memories can approach storage densities of $1/\lambda^3$, which yields storage capacities ranging from 10^{11} to 10^{13} bits/cm^3. Our design described below has a potential storage capacity of 18 GBytes (1 GByte = 10^9 Bytes) within a data storage cuvette with dimensions of 1.6 cm × 1.6 cm × 2 cm.

The goals of this research and development program were to optimize bacteriorhodopsin based photochromic and photorefractive materials for use in optical memories. Two spatial light modulators (SLMs) based on bacteriorhodopsin were developed, one which could be controlled via applied voltage and the other controlled by light. The former performed below target specification whereas the latter achieved diffraction efficiencies two-fold above target. Preliminary results on the three-dimensional data cube were sufficiently exciting to adjust the goals to also include the optimization of the bacteriorhodopsin data cube.

2. Statement of Work. The goals of the effort were to develop protocols for preparing thin films of bacteriorhodopsin for use in optical memories with reproducibility of optical quality and performance, and to verify performance by incorporating these films in two ambient temperature optical memory prototypes. Thus, the project emphasized materials development rather than prototype development. The two memory prototypes which were used to test the thin films were the ambient temperature cache memory and the Fourier transform optical associative memory. In addition, a spatial light modulator (SLM) based on bacteriorhodopsin was to be developed. The SLM is a critical component of the Fourier transform optical associative memory, and its preparation will test the ability of an oriented thin film of bacteriorhodopsin to have its photochromic and photorefractive properties controlled via applied external voltage. Success with materials development on the three-dimensional oriented bacteriorhodopsin cubes prompted the acceleration of this effort. This research was originally scheduled as a second year project.

3. Performance Analysis Table. The following table overviews the first year performance in terms of target relative to actual performance. In all but one category, performance exceeded targets. A more detailed discussion is provided in Section 4.

Performance Analysis	BELOW TARGET					ABOVE TARGET							
Principal Goals	–5	–4	–3	–2	–1	+1	+2	+3	+4	+5	+6	+7	+8
bR Thin Films													
polymer matrix optimization													
chemical additive optimization													
film preparation optimization													
holographic efficiency													
voltage controlled spatial light modulator													
bR Three-Dimensional Data Cubes													
polymer matrix optimization													
chemical additive optimization													
cube preparation optimization													
protein orientation													
photoelectrical signal													

4. Overview of Performance.

The only subproject for which we were unable to achieve the state project goals involved the development of a voltage controlled spatial light modulator. This modulator had a target characteristic of three-orders of magnitude of voltage control of the lifetime of the **M** state intermediate. In our experiments, less than one order of magnitude was achieved. This result does not indicate that a larger voltage control range is not possible, but it does indicate that our approach to this problem is not optimal. This result indicates that the Fourier transform associative memory will have a maximum reference data refresh rate of one segment per 20 milliseconds. Fortunately, our ultimate goal of making a volumetric memory based on bacteriorhodopsin is not affected by this failure.

We have had a number of key successes. The first, and most important success, has been in the development of oriented bacteriorhodopsin "cubes" with excellent and reproducible optical quality. Our experiments indicate that the nonlinear optical response of these oriented cubes is sufficiently high to permit the use of low power infrared lasers to read and write information in three dimensions at near ambient temperature. The degree of orientation approaches 100% and yields a highly reproducible photovoltage that provides unambiguous state determination of the molecules within the ($3\times3\times3$ μm^3) photochromic bit element.

Second, we have developed a method of reading and writing data within the irradiated volume of the bacteriorhodopsin cube which does not damage data cells outside of the irradiated volume. Our procedures, which are based on the use of laser "cleaning pulses", is a critical development in the implementation of a reliable two-photon based three-dimensional memory.

Third, we have arrived at a set of chemical additives that when used in combination, provide a dramatic improvement in **M** state lifetime in ambient temperature thin films, as well as the oriented protein cubes. While further improvements in the mixture are anticipated, the current formulation has proved to be adequate for a number of applications including dynamic holography, optical correlation, and as a medium in which to perform incoherent to coherent conversion.

Fourth, we have optimized the procedures for fabricating thin polymeric films containing bacteriorhodopsin. These films give excellent diffraction performance, resolution, and high sensitivity.

5. Holographic Bacteriorhodopsin Films

5-A. Thin Film Optimization. The development and characterization of bacteriorhodopsin thin films represent two significant successes for this contracting period. Many of the problems incurred during the contract have been resolved. This includes problems associated with reproducibility, diffraction performance and producing films possessing long term stability. Our film methodology, which is based on the addition of chemical agents to the native bacteriorhodopsin protein, yields **M**-thermal intermediate lifetimes ranging from milliseconds to minutes, and corresponding sensitivities that exceed those found in mutant films. Hence, with reference to the film target specifications outlined in the proposal, the current performance of our holographic thin films surpass our proposal objectives (See Table II). The procedure for making thin polymeric films of bacteriorhodopsin was developed by graduate student Richard Gross. The protocol describing the film fabrication procedure is detailed in the following subsection.

Table II. Comparison of Target versus Current Performance of Ambient Temperature Holographic Read/Write Thin Films Based on Bacteriorhodopsin

Property	Target Performance	Current Performance
film size	1 inch diameter	1 inch diameter
film thickness	50 – 200 μm	~100-200 μm
type of recording	absorption & phase	absorption & phase
diffraction efficiency (647 nm)	4.9%	6%
optical density (570 nm)	1.5 – 3.0 O.D.	.5-6.0 O.D. (pour&dry)
resolution	2000 line pairs/mm	>1400 line pairs/mm
uniformity of optical density	± 0.01 O.D.	± 0.03 O.D. (estimate only)
reciprocal sensitivity	50 mJ/cm^2	26-60 mJ/cm^2
maximum transmittance	~ 90%	99% (570 nm @700 mW/cm^2)
minimum transmittance	~ 0.3%	.2% (570 nm @ .35 mW/cm^2)
contrast ratio	~ 300	>120 (514 nm)

5-A.1. Thin Film Protocol. Purple membrane of *Halobacterium halobium*, strain S9-P is grown, isolated and purified by the procedures developed in our laboratory. For most applications, we omit the sucrose density gradient step. Instead, the purple membrane is washed and centrifuged (25K 45Ti Beckman rotor) five to six times with doubly distilled water. A 10% -15% (w/w) poly(vinyl alcohol) solution is made by dissolving 10 to 15 grams of polyvinyl alcohol (MW~20K-50K) in 85 grams of cold distilled water . This solution is heated for several hours, cooled, and then centrifuged to remove any undissolved polymer and particulate matter. The polymer solution is then made between 0% - 10%(w/w) in 1,3 diaminopropane (or 1,2 diaminoethane or 1,4 diaminobutane) and 0 to 2%(w/w) guanidine hydrochloride (or arcaine or arginine). The concentration ratio of chemical additive to protein and the humidity of the dried film directly controls the thermal decay rate of the **M**-intermediate, and consequently the photochromic properties of the protein. Sodium azide is added to the polymer solution (.05% w/w) to prevent the growth of microbes. The solution pH is then adjusted to 10.5 with hydrochloric acid and mixed thoroughly with a flea stir bar. Concentrated purple membrane [1-2 mM] is then added to the polymer solution [typically 40%-60% (w/w)] and this solution degassed for 5 minutes under high vacuum to remove air bubbles which degrade dry film quality. To assure the removal of bubbles the solution is centrifuged at 10K for 10 minutes in a Beckman 42Ti rotor. Films are cast on 1 inch BK-7 glass substrates by the pouring method [typically 500-800 μl solution on 1 inch diameter disks], or alternatively, with the use of a film casting knife. The cast films are placed in a desiccator containing a non-harsh desiccant such as silica gel and then dried for 1-3 days. After drying, the film is treated with a minute amount of glycerol (1-2 drops) and covered with a second BK-7 glass disk. The film is then placed and sealed in a specially designed air tight aluminum retainer. This process is vital to preventing film degradation caused by crystallization of the chemical agents. A picture of a film-retainer assembly prototype, and a schematic diagram of an unassembled retainer, are shown in Figure 1 and Figure 2, respectively.

5-B. Characterization and Performance Testing of Thin films. We have experimentally determined the diffraction efficiency, sensitivity, resolution, and **M**-lifetime of a series of "chemically enhanced films" containing the native bacteriorhodopsin protein, diaminopropane and guanidine hydrochloride in a poly(vinyl alcohol) matrix. Using the film

fabrication method described in the previous section, five high optical quality films of optical densities; 1.8, 2.5, 3.6, 5.4 and 5.8 were produced. Film thicknesses, as measured with a micrometer, ranged from 100 to 200 μm. A schematic diagram, and a description of the of the experimental apparatus used to quantify the properties of the thin films are shown in Figure 3. Briefly, the 570 nm laser line emitted from a Krypton ion laser was expanded and passed through an electronically controlled shutter. The timing of the opening and closing of the shutter was controlled via computer interface which was connected to a Keithley analog/digital (A/D) converter and several home-built amplifying circuits. Following the shutter, the laser light was passed through a beamsplitter where the beam was split into two coherent write beams. The two beams were redirected and combined at the plane of the film, generating a simple sinusoidal hologram on the bR film. To maximize fringe visibility, the intensities of the two beams were made equal by appropriate placement of neutral density filters. A second laser, operating at 647 nm, served as the readout beam. Its angle of incidence was adjusted to satisfy the Bragg condition for all write angles investigated. The intensities of both the transmitted and diffracted beams were monitored separately by two calibrated photodiodes (New Focus). The output of the photodiodes was coupled to the A/D converter (Keithley 500) and recorded with a personal computer. Holographic growth and decay curves at a number of write beam intensities were obtained for all of the films. The laser intensity of the read beam for all films investigated was ~1-2 mW/cm^2 The results from these experiments are shown in Figure 4.

5-B.1. Sensitivity. The sensitivity of the films was obtained by analyzing the initial region (linear portion) of the growth curves. The sensitivity, the basic material parameter used to compare among light recording materials, is defined through Equation 1 as [1]:

$$\sqrt{\eta} = I\, t\, V\, S_{bR} \tag{1}$$

where I is the write beam intensity (mW/cm^2), t is the exposure time, V is the fringe visibility (equal to 1 for all experiments) and S_{bR} is the sensitivity (units of cm^2/mJ). The sensitivity of each film was obtained by plotting the square root of the diffraction efficiency as a function of the total exposure ($I \cdot t$) received by the film as shown in Figure 5. (Note that the more commonly used reciprocal sensitivity (S^{-1}) is shown in the plots). The results are summarized in Table III. The reciprocal sensitivity of our films range from 26~60 mJ/cm^2 and appear to be much lower than films containing the wildtype protein with no chemical additives, and is slightly lower than the mutant protein D96→N [2, 3]. In order to facilitate the comparison of the photosensitivities between photorefractive crystals and bacteriorhodopsin, we adopt the photorefractive sensitivity definition, given by Gunter and Huignard [4].

$$\sqrt{\eta} = W_o\, S_{\eta_2}\, d = I\, t\, S_{\eta_2}\, d \tag{2}$$

where η is the diffraction efficiency, S is the photorefractive sensitivity (units of cm/mJ), W_o is the total write beam energy per unit area, (units of mJ/cm^2) and d is the thickness of the crystal in centimeters. The term, W_o, represents the total light exposure received by the crystal and is equal to the total laser beam power, I (units of mW/cm^2), multiplied by the exposure time, t, in units of seconds. Hence, the only difference between the two equations is the normalization of equation 2 with respect to the crystal thickness, d. Hence, to properly compare the sensitivities of the two materials, we multiplied the bR film sensitivities calculated from equation 1 by the film thickness. The film thicknesses, and the resulting reciprocal sensitivities, $S_{\eta_1}^{-1}$ of the bacteriorhodopsin films investigated are also shown in Table III. For convenience, we have also included another useful definition of reciprocal sensitivity, denoted S_{η_1} (units of mJ/cm^2) which takes into account both

the wavelength dependent absorptive properties, and the thickness of the material. It is related to sensitivity, S_{η_2}, defined in equation 2, via the following relationship:

$$S_{\eta_2} = S_{\eta_1} \alpha \tag{3}$$

where α is the absorption coefficient of the material in units of centimeters. When compared to the data given by Gunter and Huignard our data suggests that bacteriorhodopsin is significantly more sensitive than photorefractive crystals (See Table 2.5 and Table 2.6 in Reference) . This property coupled with the low cost, availability and ease at which one can manipulate the photochromic properties of the protein indicates that bacteriorhodopsin has significant potential as a an optical recording medium.

The rise time of the diffracted beam intensity is an important parameter when considering potential real-time optical data processing applications of bR films. The rise time is defined as the time necessary for the diffracted beam intensity to increase from 10% to 90% of its maximum value. From the initial (linear) part of the growth curves, we obtained the rise time of each film. These values are summarized in Table III. The relatively slow response time measured from the films may limit its application in real-time image processing. However, this limitation can be overcome by simply adapting the **M→bR** (readout wavelength 570 nm) holographic recording/readout scheme and moving to lower optical density films (.3-.8 range). Although the lack of a readout laser operating in the blue spectral region precluded testing of the **M→bR** recording approach, our recent purchase of a second Coherent Krypton ion laser will allow us to fully investigate both approaches to quantify any differences between optical recording arrangements.

5-B.2. M-thermal intermediate lifetime. The **M**-thermal intermediate lifetime of each film was ascertained via analysis of the decaying portion of the growth curves (write beams off), and by noting that the diffraction efficiency depends on the square of the number of **M** molecules. This approach is valid only when little or no photochemistry is initiated during the readout process. For hologram readout at 647 nm, this approximation is valid. Hence, by using a simplified model of the photocycle, the decay portion of the diffraction efficiency was approximated by the following equation[5]:

$$\eta(t) \alpha \exp(-2\, t / \tau) \tag{4}$$

Accordingly, we obtained the **M**-lifetime of the film by plotting $\ln[\eta(t)]$ as a function of time and evaluating the slope of the resulting curve. The results taken from all films tested are shown in Figure 6. Interestingly, the **M**-decay curves could be fit by a single exponential. This is in contrast to the bi-exponential decays observed in both the wildtype (no chemicals added) and mutant bR films[2, 3]. This observation could be due partially to photochemical erasure of the grating by the read beam, or may be attributed to the slow sampling rate (10 Hz) of the A/D converter which "missed" the initial fast thermal decay of the film.

5-B.3. Resolution The resolution of a film was determined by measuring the diffraction efficiency of one film as a function of the write interbeam angle. This parameter indicates the smallest resolvable fringe spacing that the bR film can record. The results, taken from a film of optical density 5.8 is shown in Figure 7. The resolution of film was found to exceed 1400 line pairs/mm.

We also determined the resolution of the same film during testing of the spatial light modulator (See section). For these experiments, an image of an Air Force Resolution chart was recorded by on the film using incoherent light from a white light source. The image was subsequently readout and recorded by a 35 mm camera using coherent light (λ=514.5 nm) from an Argon ion laser. Due to the finite aperture of the imaging lenses, the image recorded by the film was demagnified to .4 of its initial size. The highest resolvable group was found to be group 5 element 3 which corresponds to a resolution of ~ 100 line pairs/mm, after correcting for demagnification. The measurement of this value was limited only by the resolution of the imaging lenses which were ordinary 35 mm camera lenses. A photograph of the image read out from the film is shown in Figure 13.

5-B.4. Contrast Ratio The contrast ratio of the film was measured by bleaching a portion of the film (OD = 5.8) with filtered green light from a 1000 W tungsten lamp and measuring the relative absorbance of a weak probe beam at 514 nm in each area of the film. This number was found to be ~120.

Table III. Summary of Experimentally Measured Parameters

Film	Thickness (μm)	α @568nm (cm^{-1})	η_{max} (%)	τ (sec)	S_{bR}^{-1} (mJ/cm^2)	$S_{\eta_2}^{-1}$ (mJ/cm)	$S_{\eta_1}^{-1}$ (mJ/cm^2)	t_{rise} (s)	Laser Intensity (mW/cm^2)
I	~100	415	1	11.1	26	.26	6×10^{-4}	3	.15 - 1.2
II	~140	411	3	24.8	24	.36	9×10^{-4}	1.5	.25 - 1
III	~190	412	3.5	16.1	51	1.0	2×10^{-3}	2.6	.5 - 2.0
IV	~300	415	6	6.7	60	1.8	4×10^{-3}	4.4	2.1 - 5.2
V	~325	411	5.5	14.2	48	1.6	4×10^{-3}	5.5	.5 - 2.6

5-C. Chromophore Substituted Bacteriorhodopsin Analogs. We have successfully begun to prepare analogs of bacteriorhodopsin based on the use of the artificial chromophore all-trans 4-keto-retinal. This choice is based on the work of Druzhko and Zharmukhamedov who demonstrated that this chromophore provides more than a hundred-fold increase in **M** state lifetime relative to the native chromophore. As stated in last years report, the main hindrance in preparing large quantities of the bR analog material for use in thin and optical memories derives from the absence of sufficient quantities of the 4-keto retinal chromophore. We have addressed this situation by initiating a collaboration with Professor James Kallmerten, a synthetic chemist in the chemistry department. Accordingly, we expect sufficient quantities of the 4-keto retinal analog in the next 6-8 months.

5-D. Demonstration of Target Recognition (Optical Correlation) The optical design of the bench target recognition device used the dual-joint transform optical architecture first implemented by Lee and coworkers [6]. Very recently, Hampp and coworkers showed the potential of this design by demonstrating pattern recognition and real-time target tracking using mutant bacteriorhodopsin films as the optical recording medium in the Fourier plane [7]. The

advantages offered by this arrangement stem from ease of system alignment when different wavelengths are used to write and read the hologram, and the less stringent requirements of the Fourier transforming lenses [8]. The bench layout of the correlation device is shown schematically in Figure 8. Laser light (568 nm) from a krypton ion laser was passed through a fifty/fifty beamsplitter generating two coherent write beams. Both beams were redirected towards the plane of the film by means of simple mirrors and linearly polarized by Glan-Taylor polarizers (Optics For Research #PH-10). The interbeam angle of the write beams was calculated to be 16 degrees. Each beam was circularly polarized, in opposite directions, by proper rotation of quarter wave plates (Optics For Research #RM-1/4-570). This polarization recording method provided the means of separating the desired diffracted light from the unwanted scattered light noise. After circular polarization, the beams were expanded by lenses L1 and L2 (focal length 36 mm). Plano convex lenses, FT1 and FT2 (focal length 300 mm), served to Fourier transform the input and reference image transparencies. Hologram formation in the bR film used **bR** to **M** recording and non-destructive readout wavelength of 647 nm. A second krypton ion laser served as the source of the readout beam and was coupled into the correlator by means of a second beamsplitter (BS2). Its angle of incidence was adjusted to satisfy the Bragg condition. The polarization of the readout beam was made linear through the use of a simple polarizer. **M** to **bR** recording or reconstruction using wavelengths in the blue spectral region could not be tested since our readout laser could only lase in the red. The diffracted wave, which contained the desired correlation signals, was Fourier transformed with a third lens and imaged onto a CCD camera (Model SSC-C350;Sony Inc.). An interference filter placed in front of the CCD camera served to filter out the transmitted write beams. A linear polarizer, positioned just before the entrance of the camera, was used to discriminate the diffracted light from the unwanted scattered noise. All transparencies were recorded on high contrast lithographic film. The linear dimensions of the transparencies were ~ 12 mm x 12 mm.

5-D.1. Demonstration of Target Recognition The first experiment demonstrating target recognition compared a single letter transparency containing the letter A with a reference transparency consisting of the four letters P, A, S, A. Figure 9 is a photograph taken from the from CCD TV monitor that shows the transparencies used and the resulting correlation peaks. The second experiment compared a two letter input containing the letters A and P with a six letter reference transparency composed of the letters A, P, Z, G, A, G. These transparencies and the corresponding correlation peaks are shown in Figure 10. The optical density of the film used in both experiments was ~ 2.5. The total laser intensity (measured before the transparencies) was .09 mW/cm^2 and 1.5 mW/cm^2 in the first and second experiments, respectively. The laser intensity of the readout beam was identical in both experiments and was measured to be 1.5 mW/cm^2. The signal to noise ratio was estimated to be ~20:1.

5-E. Development of spatial light modulator. In 1990, we proposed the design of an electrically addressed spatial light modulator prototype [9]. After much work, which included the construction of a high voltage cell to apply electric fields $>10^7$ V/m across a bR thin film, we conclude that an electric field will not provide sufficient prolongation of the **M**-thermal intermediate. Thus, modulation of the transmission properties of a film bR by application of an electric field perpendicular to the film plane have not been successful. We have, however, recently designed and performed preliminary measurements on an optically addressed spatial light modulator that functions as an incoherent to coherent light converter. This device exploits both the high sensitivity, inherent in a chemically enhanced film, and the large shift in absorption maximum between the **bR** and **M** states to allow for incoherent to coherent light conversion. This work was performed in a continuing collaboration effort with Professor Q.W. Song from the Department of Electrical Engineering at Syracuse University. A schematic diagram and a general description of

the device is given in Figure 11. Our initial results showing the transmission properties and resolution of the SLM are given in Figure 12 and Figure 13, respectively.

6. bR Three-Dimensional Data Cubes.

6-A. Introduction

Bacteriorhodopsin has four characteristics that combine to enhance its comparative advantage as a non-linear optical photochromic medium . First, the protein has a large two-photon absorptivity due to the highly polar environment of the protein binding site and the large change in dipole moment that accompanies photoexcitation. Second, bacteriorhodopsin exhibits large quantum efficiencies in both the forward and reverse direction. Third, the protein gives off a fast electrical signal when light activated that is diagnostic of its state (see Figure 14), Fourth, the protein can be oriented in optically clear polymer matrices permitting photoelectric state interrogation. The two-photon induced photochromic behavior is summarized in the scheme below.

$$\mathbf{bR}\ (\textit{State 0})\ (\lambda_{max} \cong 1140\ \text{nm}) \underset{2h\omega;\ \Phi_2>0.65}{\overset{2h\omega;\ \Phi_1\sim0.65}{\rightleftharpoons}} \mathbf{M}\ (\textit{State 1})\ (\lambda_{max} \cong 820\ \text{nm})$$

We arbitrarily assign **bR** to binary state 0 and **M** to binary state 1. The light absorbing chromophore in **bR** has an unusually large two-photon absorptivity ($\delta = 290 \times 10^{-50}$ cm^4 sec molecule^{-1} photon^{-1}), a value which is approximately ten times larger than absorptivities observed for other polyene chromophores. This property permits the use of much lower intensity laser excitation to induce the forward photochemistry. The above wavelengths are correct to only ±40 nm, since the two-photon absorption maxima shift as a function of temperature and polymer matrix water content.

The schematic design of the two-photon three-dimensional optical memory is shown in Figure 15. Bacteriorhodopsin, housed in a sealable cuvette, is oriented by applying a small electric field prior to polymerizing the acrylamide/bis acrylamide monomers. Orientation is a prerequisite in order to use the photoelectric signal to monitor the state of the proteins occupying the irradiated volume. A write operation is carried out by firing simultaneously the two 1140 nm lasers (to write a 1) or the two 820 nm lasers (to write a 0). To eliminate unwanted photochemistry along the laser axes, nonsimultaneous firing of the lasers not used in the original write operation is carried out immediately following the write operation. This clean pulse operation is necessary since some photochemistry is initiated outside the irradiated volume. Figure 15g shows the calculated probability of two-photon induced photochemistry as a function of location relative to the center of the irradiated volume. As can be seen from an analysis of Figure 15g, photochemistry occurs outside of the irradiated volume along the laser beam axes. Nearby memory cells along the laser axes are transformed to a (worst case) ~25% of the irradiated volume (desired memory cell) transformation, and repeated read/write operations may irreparably destroy the contents of unaddressed memory cells after multiple write operations. This problem can be minimized by adjustment of the clean pulse intensity or laser pulse duration. A computer simulation showing the result of the cleaning operation in an irradiated volume is shown in Figure 15e. The cleaning operation serves to reduce unwanted photochemistry from ~25% to ~2%, the latter level being more than adequate to maintain data integrity outside of the irradiated volume. The entire write operation, including the subsequent cleaning pulses, can be completed in less than 50 ns.

Two-photon induced photovoltage is used to read the information stored in 3-D memory. By firing all four lasers simultaneously, the state of the irradiated volume can be probed by monitoring the photovoltage. If α-β is negative, then the memory cell defined by the irradiated volume is in the 0 state. If α-β is positive, then the memory cell defined by the irradiated volume is in the 1 state. (Note that we arbitrarily assign the voltage signs as shown in Figure 14). Careful adjustment of the relative intensities of the four lasers permits minimal disturbance of memory cells outside of the irradiated volume. A standard write operation is then performed to reset the memory cell to the correct state. This procedure serves to enhance data integrity by reducing the risk that multiple read/write cycles along the axis occupied by the interrogated memory cell corrupt the data in that memory cell. The total read process can be completed in ~50 ns, which means that the maximum serial data rate is ~20 Mbit/s. This data rate is decreased by the time necessary to move the cube to the next memory cell. This latency is determined by the extent to which the data to be read are contiguous and by the translation actuators. The position of the cube is controlled in 3-dimensions by using a series of actuators which independently drive the cube in the x, y or z direction with a high-resolution stepper motor driven micrometers.

The use of bacteriorhodopsin in two-photon based three-dimensional memories requires the development of polymer cubes rather than polymer thin films. These cubes must have high optical homogeneity and clarity while maintaining the requisite two-photon absorptivity of the component protein. In addition, bR must be oriented in a polymer matrix in order to use two photon induced photo voltage to perform the read operation. As noted in brief below, we have developed a protocol for preparing oriented bacteriorhodopsin cubes which yield excellent photoelectric performance under excitation conditions that suggest that our storage medium is capable of high density three dimensional storage. We have also developed excitation protocols that permit read and write operations that do not destroy data outside of the irradiated volume.

6-B. Polymer matrix optimization. Three different polymer matrices have been tested for use in generating cubes of oriented bacteriorhodopsin: (a) methyl cellulose, (b) polyacrylamide and (c) bovine gelatin. We know from previous studies on the thin films that polyvinyl alcohol does not yield high quality thick films, and is thus not a useful polymer for the present application. Although bovine gelatin and methyl cellulose both produce very stable cubes, neither yields the excellent optical quality that is routinely achieved by using polyacrylamide. We have decided to limit our investigations to the optimization of polyacrylamide based polymer matrices and have developed a protocol to make oriented bR cubes with polyacrylamide polymer as a host matrix.

6-C. Chemical additive optimization. To enhance **M** state lifetime we have investigated the following chemicals; 1) guanidine hydrochloride, 2) ethylene diamine, and 3) diamino propane. Our results indicate that these chemical additives have a strong effect on the **M**-thermal intermediate lifetime. Although the exact chemical or physical origin of these effects are unknown, it is clear that these effects are enhanced when the pH of the bR solution is high (around 9.5 to 10.5). We also found that adding a small amount of sodium azide (0.6% by weight) is necessary to prevent the growth of organisms.

6-D. Cube preparation optimization. We have developed the following protocol for preparing the polymer matrix. The purified purple membrane is first washed 5-6 times with doubly distilled water to reduce the conductivity of the solution. This process minimizes the electrolysis of water at the electrode/solution interfaces. The purple membrane is then passed through a 5 μm pore size filter to remove particulate matter. Concentrated bR is then diluted with the acrylamide and N,N'-methylene-bis-acrylamide to a final protein concentration of ~ 300μM (absorbance at 570 nm adjusted to 8-10). Additional chemicals can be added at this stage to control **M** state lifetime if desired (see below). Polymerization of 300 μM of protein in 30% acrylamide

and 0.8% bis-acrylamide is catalyzed with 1.5% ammonium persulfate and initiated by TEMED {N,N,N'N' tetramethylethylenediamine} in order to complete homogeneous polymerization within 10 minutes, and to avoid the negative consequences of self-heating due to free radical formation. A second method is also used which employs 0.2% riboflavin as the catalyst and polymerization is initiated by a uv lamp. The first method is preferred under most circumstances because it is faster and more easily implemented. The polymerization and electrophoresis is carried out in an home built electrophoresis chamber. An example of one chamber that is used consists of a Teflon base (4 cm x 1.6 cm) with platinum electrodes on both sides (see Figure 16). A voltage (20 V/cm) is used to orient the purple membrane sheets of bacteriorhodopsin. The duration of the applied voltage ~30 s and is timed to occur just prior to polymerization. Because the polymerization time depends on many factors including temperature, protein concentration, and oxygen in the solution, we first determine this parameter by polymerizing a small quantity of the same mixture. The bR cubes produced by these methods contain protein that is highly oriented with the cytoplasmic side facing the anode (cytoplasmic side charge = ~-3). After polymerization was complete, deionized water is poured into the chamber to cool the gels. This step is critical to the quality of the gel because excessive heat will denature the protein. bR cubes produced by these methods contain protein that is highly oriented. However, some nonuniformity is observable in the gels produced with d.c. electric fields. This nonuniformity is due to the negative charge that the purple membrane carries. The membrane patch aligns with the electrical fields and also migrates toward the anode. The migration is responsible for the non-uniformity because the speed of migration is proportional to the size of the purple membrane sheet. This problem can be solved by using short voltage pulses for protein orientation.

6-E. Incorporation of oriented gels into photoelectric cells We have designed and constructed a photoelectrical cell holder. The gel holder is a cuvette with two opposite faces inside the cuvette coated with a thin conductive transparent layer of indium tin oxide as shown in Figure 17. A small circular hole is drilled in one face of the cuvette to mount an SMA connector, which serves to connect the electrode faces with an external measuring device. Although regular glass cuvettes are commercially available, no vendors could supply a cuvette with conductive coatings on opposite faces inside cuvette. We attempted to sputter a thin transparent layer of nickel onto the internal faces of a quartz cuvette. The small cuvette dimensions, however, (which are necessary for observing the photoelectric signals from the bR cube) precluded homogenous deposition, and was not successful. We solved this problem by sputtering conductive coating on a glass substrates, then assembling the glasses into an cuvette with epoxy.

Before incorporating the oriented gels into photoelectric cell, the gel is carefully removed from the electrophoresis chamber and bathed in 100 mM potassium chloride for 24 hours. The gel slab is then cut into cubes that fit into the photoelectrical cell holder. The gel is sealed from the outside environment by applying a layer of silicon or epoxy to the top of the gel holder. The sealing is necessary to avoid gel dehydration.

6-F. Characterization of prototype two-photon three-dimensional memory Our design of the bR based two-photon three-dimensional memory uses two-photon absorption to write and two-photon induced photovoltage to read information. Bacteriorhodopsin has a large two-photon absorption cross section which has been measured previously[10]. Although two-photon induced photovoltages has been observed in dried bR thin films, these signals have never been measured for a cube larger than 1 cm^3. Since the photoelectrical signal is inversely proportional to the separation of the two electrodes, the signal from a thick gel is expected to be much smaller in magnitude than those observed in thin films. The most important task for this 3-D device is to test whether signal of the two-photon induced photoelectrical signal from a bR cube is large enough to be used to assign state. In addition, two-photon induced photoelectrical signal is

also an indication that the bR molecules are pumped to the K state (which will then decay to the M state). We have demonstrated that a strong photoelectrical signal can be observed in a bR cube with a dimension of 1.6x1.6x1.6 cm.

6-F.1. Two-photon induced photoelectrical signal A key performance test for the oriented cube is the measurement of the two-photon induced photoelectric signals. Figure 18 shows a schematic diagram of the experimental apparatus used to measure the read/write capabilities of the two-photon three-dimensional memory. A 1.06 μm beam from a Q-switched YAG laser with a repetition rate of 10 Hz and a pulse width of 10 nsec was used as the light source (DCR-2 from Spectra Physics). A beam attenuator (specially designed and constructed by Newport) was used to modulate the laser light intensity without shifting the beam position. The bR cube was mounted on a precision x-y-z stage which was controlled via stepping motors interfaced with a microprocessor (ATS 302 from Aerotech). The photoelectrical signal was recorded with a 250 MHz bandwidth digital oscilloscope (HP54510A). To prevent inductive pick up of electrical noise from the Q-switch of the Nd:YAG laser, the cell holder and all the cables were shielded with a conductive copper mesh.

The measured two-photon induced photovoltages for different laser pulse energies are shown in Figure 19. Most significant is the observation that the two-photon induced photovoltage is detectable for laser energy densities as low as 15 mJ/cm^2. Noise in the signal stems primarily from inductive coupling of the high voltage Q-switch pulse to the photoelectric cell. This noise can be minimized if a proper shielding is applied. All of the signals shown in Figure 19 use no amplification. Photovoltages as high as 2 mV has been observed for energy densities of 150 mJ/cm^2. The signal to noise ratio of the read system can be dramatically improved if an amplifier circuit is built into the photoelectrical cell. This design will be implemented in our second generation prototype. For comparison, we also measured the one photon induced photovoltage excited by the 0.532 μm second harmonic beam of the Nd:YAG laser and the results indicate that the signal profile is identical to that observed via two-photon excitation within experiment error.

The profile of the photoelectrical signal from the gel cube is significantly different than those derived from oriented dried films of bacteriorhodopsin. The photoelectrical signal from dry film has two components, one fast and one slow components (labeled α and β in the diagram). However, Only the fast component is observed in the gel cube. Although exact mechanism requires further investigation, the disappearance of the slow components is probably due to the ion diffusion which cancel the slow components of the signal. When the slow component is present, state assignment from two-photon induced photovoltage requires discriminating the two components in real time. Therefore, the disappearing of the slow components simplified the reading processing significantly. The pulse width of the signal is less than 20 nsec.

6-F.2. Write/read speed The fast two-photon induced photovoltage in Figure 19 indicates that the read speed of the memory is on the order of 30 nsec. The write speed can also be derived from the recorded photovoltage signal. As is well known for the bR photocycle, once ground state bR molecules are photoactivated to the **K** state, it will decay to M state without any photon energy. Although switch time between **bR-M** takes about 50 μsec, our photoelectrical signal results indicate that the actual laser pulse required to initiate the transition is less than 30 nsec. Thus, the intrinsic limitation of the read/write speed is 30 nsec. This speed is much higher than any optical access method currently available. The speed of the 3-D memory will be limited by the optical access time rather than by the materials response. At present, we use a stepping motor driven x-y-z stage (Aerotech, ATS302) which has a resolution of 0.1 μm and an access time of 250 μsec for a bit size of 1μm. Mechanical actuator with access time of as fast as 5 μsec are commercially available (Aerotech, ATS400 series). The cost of such a actuator is on the order of $10,000.

However, the high price of the actuator is partially due to the small market. A specially designed 3-D actuator for the 3-D memory would be more compact and less expensive. Alternatively, we can also steer the beams to access the data stored in the cube. For example, a dynamic focusing lenses (DFL), such as electrooptical DFL and holographic DFL, can be used to access information .

6-F.3. Damage threshold of bR bR is a robust molecule. The photocyclicity has been measured to be better than 10^6 [11, 12]. However, the laser damage threshold has not been evaluated. Since two-photon process depends quadratically on the laser intensity, high peak power laser beam must be used. The laser damage threshold is an important parameter for evaluating the efficacy of the three dimensional memory. We tested damage threshold of the bR cubes. For a 532 nm green beam of the YAG laser, permanent bleaching of the protein is observed when the peak intensity of the laser is greater than 2.5 MW/cm^2. However, for 1.06 μm IR beam of the YAG laser, no damage is observed for laser peak intensity as high as 10 MW/cm^2. Since all the lasers used for read and write in our two-photon 3-D memory are IR beam, the laser induced damage would not be a problem for laser peak intensity below 10 MW/cm^2.

6-F.4. Signal to noise ratio The signal to noise ratio of the two-photon induced photovoltage depends on the excitation light intensity. For laser pulse energy density of 150 mJ/cm^2, the signal to noise ratio is larger than 20 after background subtraction. However, for laser pulse energy density of 15 mJ/cm^2, the signal to noise ratio is only 4. As indicated previously, noise originates primarily from inductive coupling of the electromagnetic radiation from the high voltage pulse of the Q-switch of the Nd:YAG laser to the photoelectric cell. Copper mesh has been used to shield both the cable and cell from the inductive coupling in our experiments. This technique proved to be very effective and the background noise after shielding was reduced by at least a factor of 4. The noise level floor is on the order of ~50 μV after shielding. We should point out that no amplifier circuit is used. The signal to noise ratio could be improved significantly if an amplify circuit were built into the base of the cell and the whole unit were shielded. This design will be implemented in the second generation prototype.

6-G. Conclusion We have successfully constructed an oriented bR cube for three-dimensional optical storage. Write/read capability is demonstrated by the photoelectrical signal induced by two-photon absorption. Although the two-photon induced photoelectrical signal has been observed in thin films of oriented bR, this is the first time such signals have been detected in a three dimensional cube as large as 1.6x1.6x1.6 cm. The intrinsic limitation of the material response of the write/read speed is determined from the two-photon signal to be 30 nsec. This speed is much higher than any optical access technology currently available. Therefore, the speed of the memory will be limited by the optical access time rather than by the material response. Although significant progress has been made in the materials aspects of this memory storage approach, further research and development is still required to realize its potentials.

References:

1. Collier, R. J., C. B. Burckhardt and L. H. Lin. 1971. Optical Holography. Academic Press, New York.

2. Hampp, N., A. Popp, C. Brauchle and D. Oesterhelt. 1992. Diffraction efficiency of bacteriorhodopsin films for holography containing bacteriorhodopsin wildtype BRwt and its variants BR_{D85E} and BR_{D96N}. *J. Phys. Chem.* 96: 4679-4685.

3. Hampp, N., C. Bräuchle and D. Oesterhelt. 1990. Bacteriorhodopsin wildtype and variant aspartate-96 → asparagine as reversible holographic media. *Biophys J.* 58: 83-93.

4. Gunter, P. and J. P. Huignard. 1988. Photorefractive Materials and Their Applications I. *In* Photorefractive Materials and Their Applications I: Fundamental Phenomenon. P. Gunter and J. P. Huignard, eds. Springer-Verlag, New York. 8-73.

5. Brauchle, C. and D. Burland. 1982. Holographic methods for the investigation of photochemical and photophysical properties of molecules. *Angew. Chem. Int. Ed. Engl.* 22: 582-598.

6. Lee, T. C., J. Rebholz and P. Tamura. 1979. Dual-axis joint transform correlator. *Opt. Lett.* 4: 121-123.

7. Thoma, R. and N. Hampp. 1992. Real-time holographic correlation of two video signals by using bacteriorhodopsin films. *Opt. Lett.* 17: 1158-1160.

8. Joyeux, D. and S. Lowenthal. 1982. Optical Fourier transform: what is the optimal setup? *Appl. Opt.* 21: 4368-4372.

9. Birge, R. R., P. A. Fleitz, R. B. Gross, J. C. Izgi, A. F. Lawrence, J. A. Stuart and J. R. Tallent. 1990. Spatial light modulators and optical associative memories based on bacteriorhodopsin. *Proc. IEEE EMBS.* 12: 1788-1789.

10. Birge, R. R., P. A. Fleitz, A. F. Lawrence, M. A. Masthay and C. F. Zhang. 1990. Nonlinear optical properties of bacteriorhodopsin: assignment of second order hyperpolarizabilities of randomly oriented systems using two-photon spectroscopy. *Mol. Cryst. Liq. Cryst.* 189: 107-122.

11. Chen, Z., A. Lewis, H. Takei and I. Nabenzahl. 1991. Bacteriorhodopsin oriented in polyvinyl alcohol films as an erasable optical storage medium. *Appl. Opt.* 30: 5188-5196.

12. Oesterhelt, D., C. Brauchle and N. Hampp. 1991. Bacteriorhodopsin: a biological material for information processing. *Quart. Rev. Biophys.* 24: 425-478.

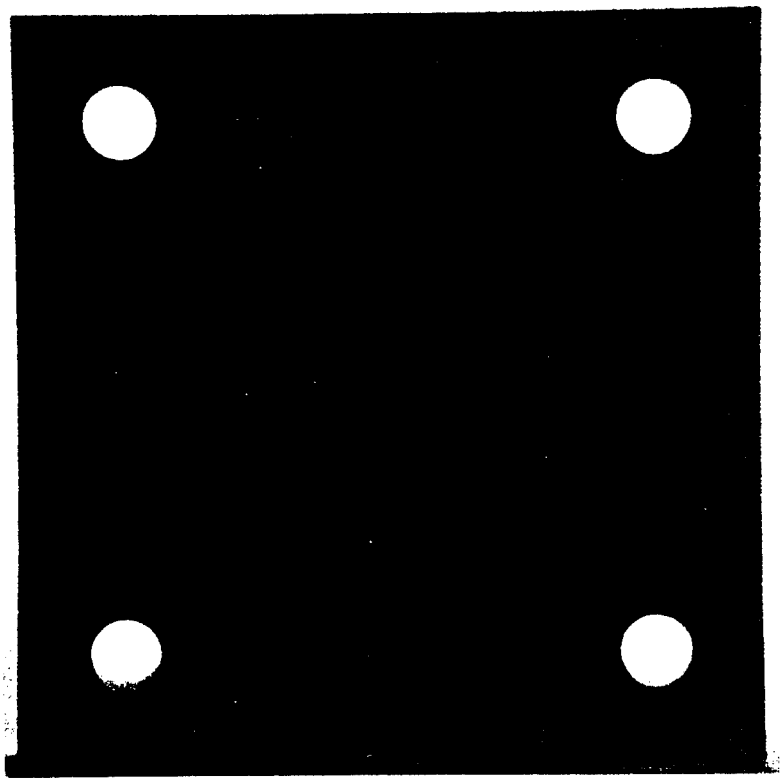

Figure 1: A picture of a thin chemically enhanced film of bacteriorhodopsin housed in an anodized aluminum film retainer. The retainer provides an air resistant seal which prevents film degradation due to crystallization of the chemical additives.

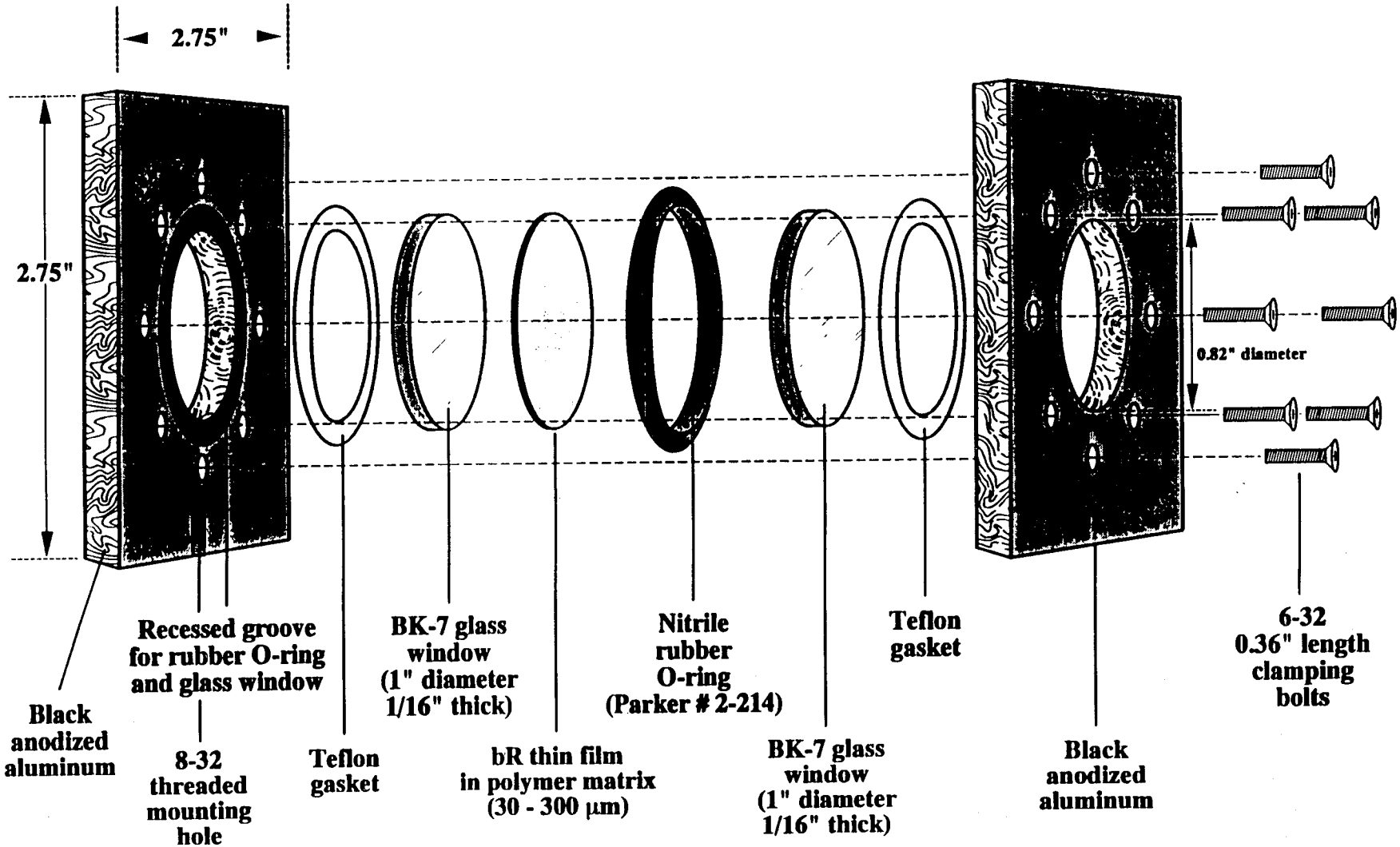

Figure 2: Schematic diagram of the air-tight aluminum retainer used to seal a chemically enhanced film of bacteriorhodopsin from the outside environment.

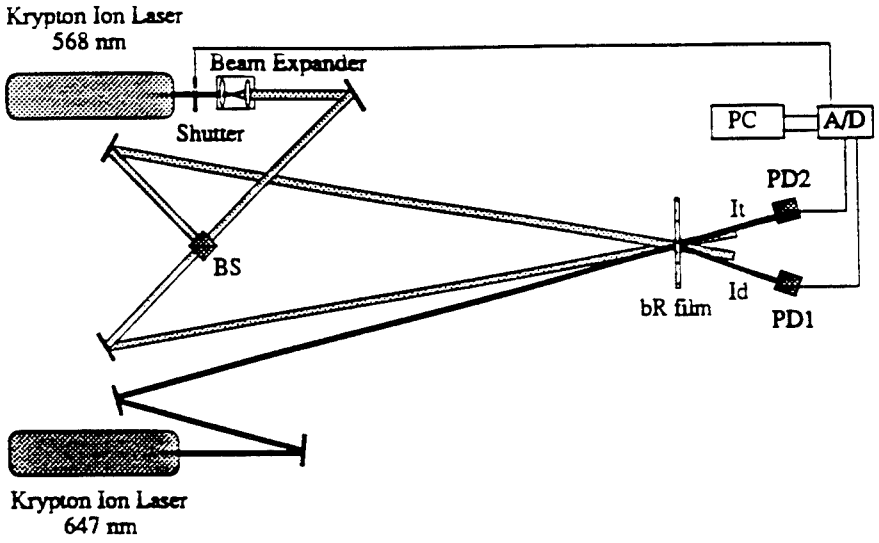

Figure 3: Experimental apparatus used to characterize the holographic properties of bacteriorhodopsin films. The 570 nm laser line emitted from a Krypton ion laser was expanded and passed through an electronically controlled shutter. The timing of the opening and closing of the shutter was controlled via computer which was interface to a Keithley analog/digital (A/D) converter and several home-built amplifying circuits. Following the shutter, the laser light was sent through a beam splitter [BS] where the beam was divided into two coherent write beams. The two beams were redirected via simple mirrors and combined at the plane of the film thereby generating an interference grating on the film (See text). To maximize fringe visibility, the intensities of the two beams were made equal by the appropriate placement of neutral density filters. A second laser, operating at 647 nm, served as the readout beam. Its angle of incidence was adjusted to satisfy the Bragg condition for all write angles investigated. The intensities of both the transmitted and diffracted beams were monitored separately by two calibrated photodiodes [PD1 and PD2]. The output of the photodiodes was coupled to the A/D converter [A/D] and recordeded by a computer [PC]. The laser intensity of the read beam for all films investigated was ~1-2 mW/cm^2.

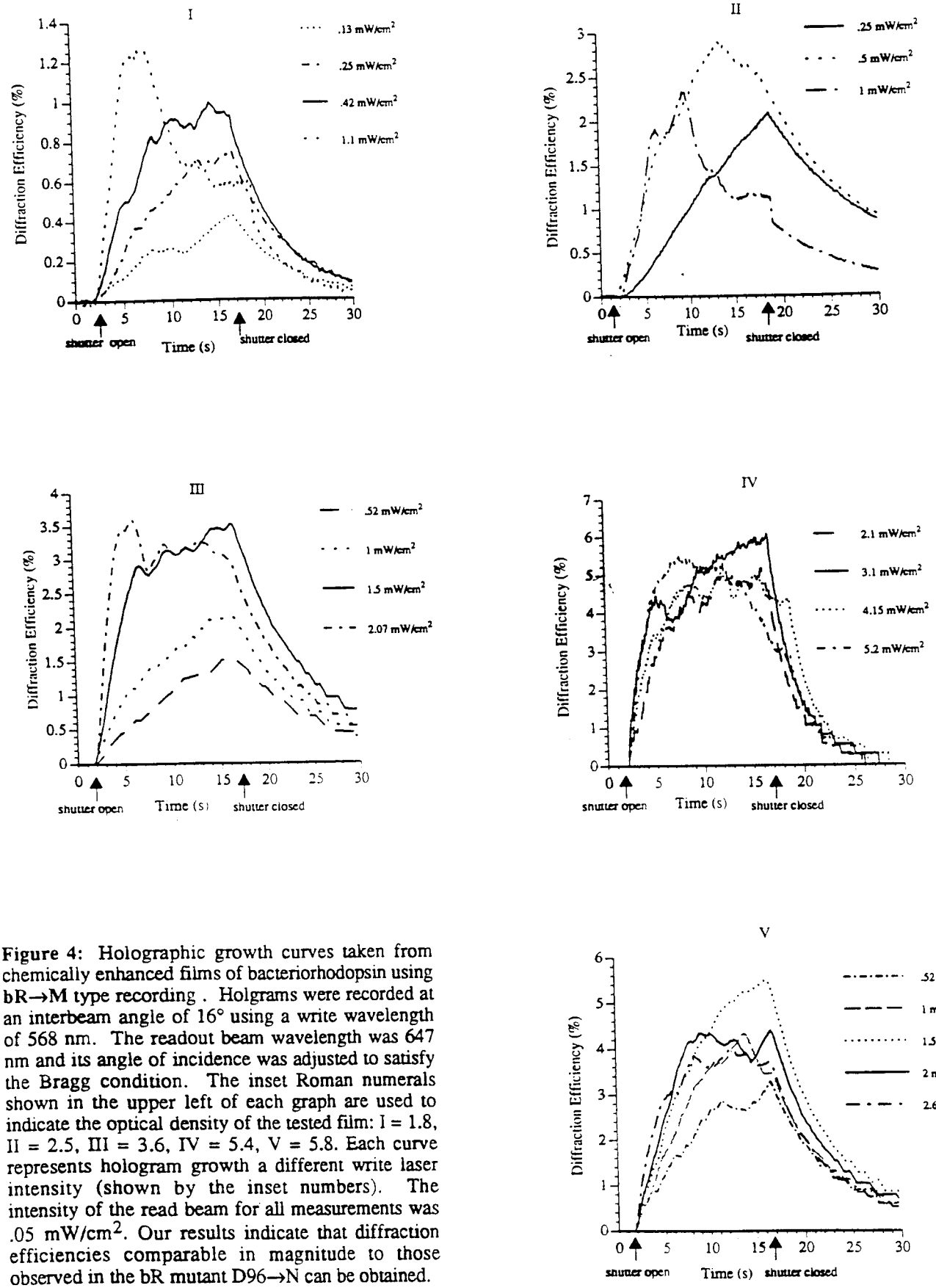

Figure 4: Holographic growth curves taken from chemically enhanced films of bacteriorhodopsin using **bR→M** type recording . Holgrams were recorded at an interbeam angle of 16° using a write wavelength of 568 nm. The readout beam wavelength was 647 nm and its angle of incidence was adjusted to satisfy the Bragg condition. The inset Roman numerals shown in the upper left of each graph are used to indicate the optical density of the tested film: I = 1.8, II = 2.5, III = 3.6, IV = 5.4, V = 5.8. Each curve represents hologram growth a different write laser intensity (shown by the inset numbers). The intensity of the read beam for all measurements was .05 mW/cm^2. Our results indicate that diffraction efficiencies comparable in magnitude to those observed in the bR mutant D96→N can be obtained.

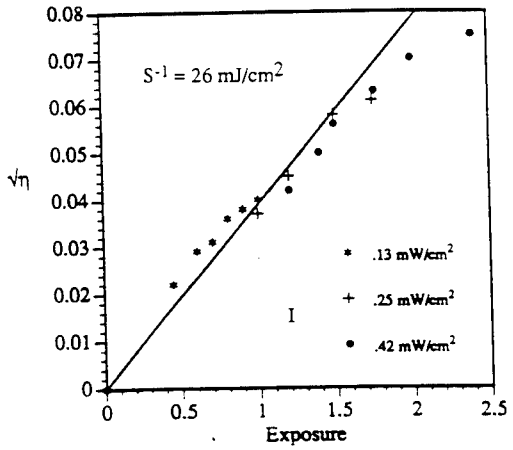

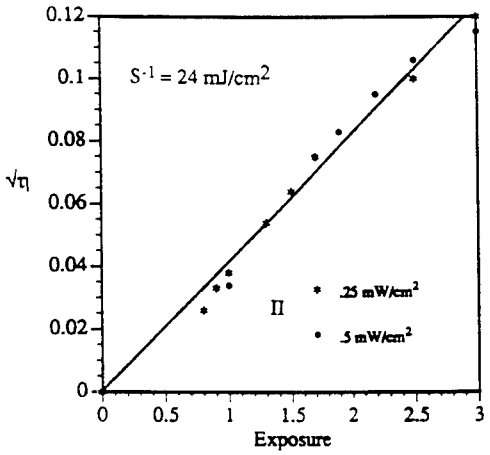

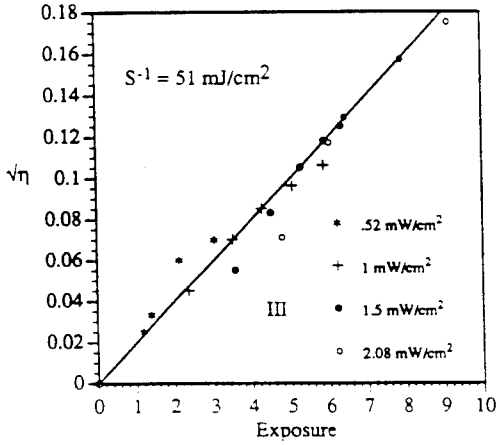

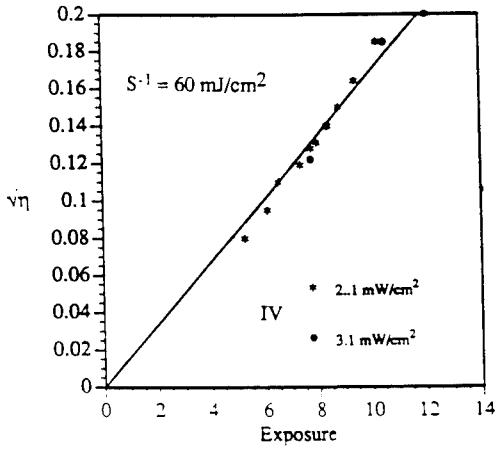

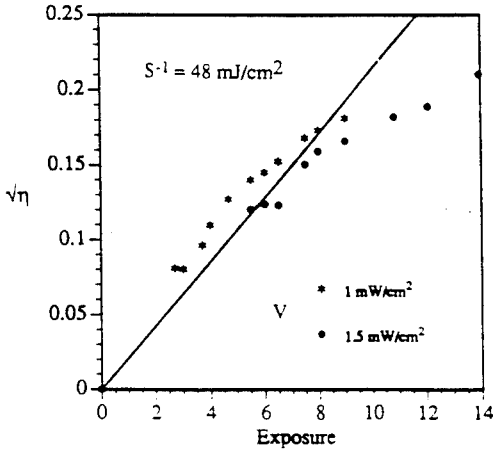

Figure 5: Sensitivity curves derived from the decaying portion of the holographic growth curves. Each graph represents a film of varying optical density I = 1.8, II = 2.5, III = 3.6, IV = 5.4, V = 5.8 and chemical composition. Sensitivities were calculated by use of Equation 12 and are reported in the graph using the traditionally used reciprocal form, S^{-1}. Data points taken at different laser intensities show reasonably good correlation. The sensitivities (range 20-60 mJ/cm^2) of chemically enhanced bR films appears to be lower than similar films containing either the wildtype or D96→N mutant protein.

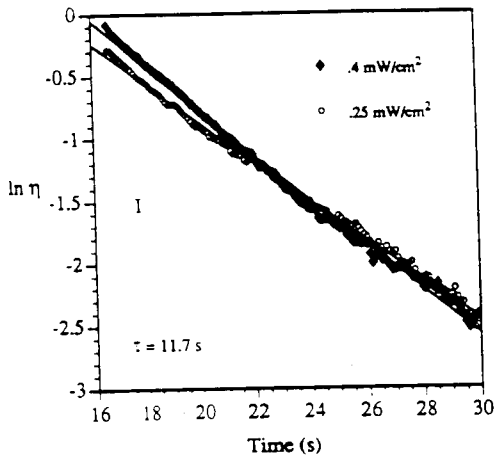

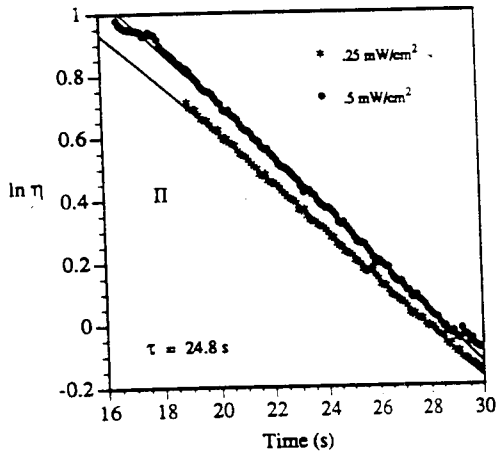

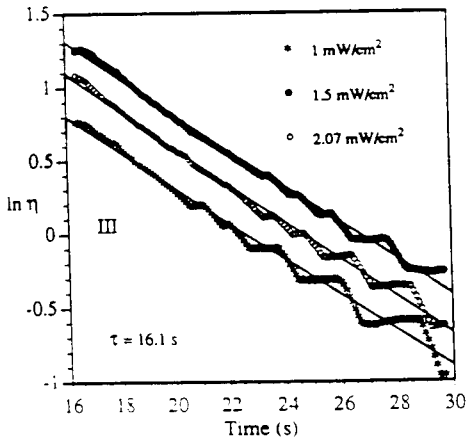

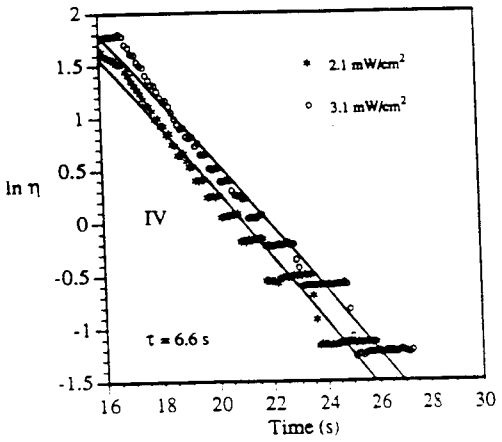

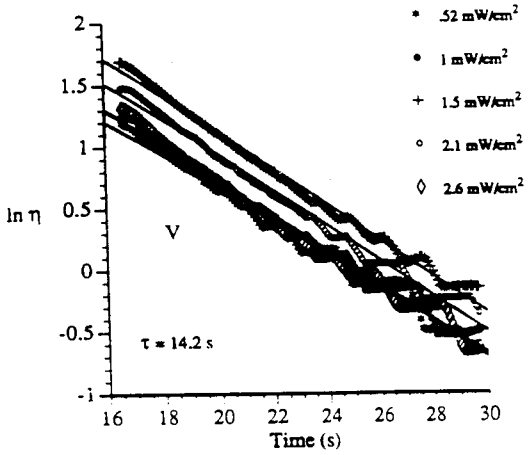

Figure 6: The thermal decay of the **M**-intermediate in chemically enhanced films obtained by plotting the ln η as a function of time (write beams off: See Equation 13). Each graph represents a film of varying optical density and chemical composition: I = 1.8, II = 2.5, III = 3.6, IV = 5.4, V = 5.8. Interestingly, the data can be fit by a straight line. These results suggest that the **M** thermal decay in chemically enhanced films differs from that observed in films containing the wildtype (containing no chemicals) or mutant protein (bi-exponential decay). The data also shows that considerable flexibility in controlling the **M**-lifetime of the film can be maintained using the chemical approach.

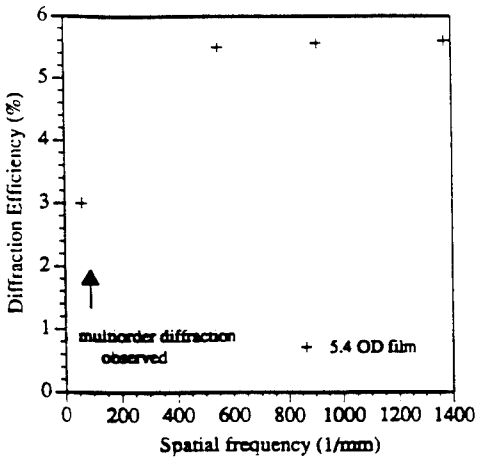

Figure 7: The spatial resolution measured from one film of bacteriorhodopsin (OD ~ 5.4, thickness ~175 μm) by varying the interbeam angle of the write beam (writing wavelength of 568 nm) (See text). This procedure indicates the interference fringe spacing that the film can resolve. The spatial frequency, υ, of the fringe pattern is related to the write interbeam angle (2ϕ) and the wavelength of the write beam via the relation $\upsilon = 2 \sin(\phi)/\lambda_w$. Multi-order diffraction was observed at small recording angles.

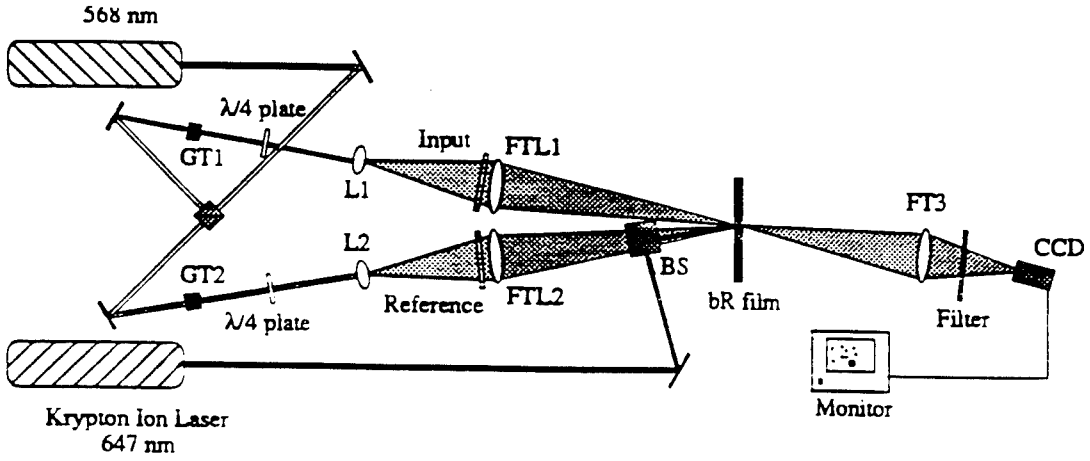

Figure 8: Schematic diagram of the dual-joint transform correlator used to perform target recognition based on a chemically enhanced bacteriorhodopsin film in the Fourier plane. Polarization recording was implemented by passing the write beams through Glan-Taylor linear polarizers [GT1 and GT2] and quarter wave plates. Plano convex lenses were used to expand the beam prior to Fourier transformation [L1 and L2] Post-lens Fourier transformation of the input and reference images was realized with 300 mm plano- convex lenses [FTL1 and FTL2]. A beam splitter served to couple the readout beam (647 nm) into the device. The diffracted correlation signals were separated from the write beam by means of an interference filter placed before the entrance to the CCD camera. The correlation procedure used steady state diffraction from the bR film (write and read simultaneously). The laser intensities of the write and read beams were ~.1 and 1.5 mW/cm^2, respectively.

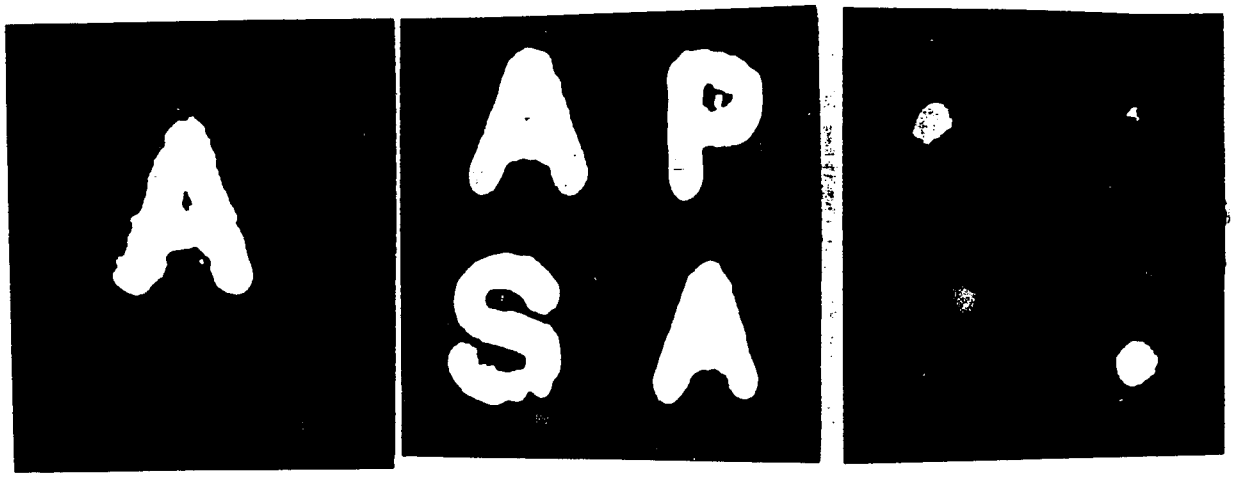

Figure 9: Pictures taken from the CCD TV monitor demonstrating pattern recognition using a chemically enhanced bR film in the Fourier plane. The input image (left) containing the single letter A is cross correlated with the 4-letter reference image (middle) containing the letters A, P, S, A. The right picture shows the resulting cross correlation signals diffracted from the bR film. The intensity or brightness of the spots indicate the degree of likeness between the input and reference images, and gives the corresponding spatial location with regard to the reference image. The linear dimensions of the transparencies were ~12 mm x 12 mm. The optical density and thickness of the film was 2.5 and 100 μm, respectively.

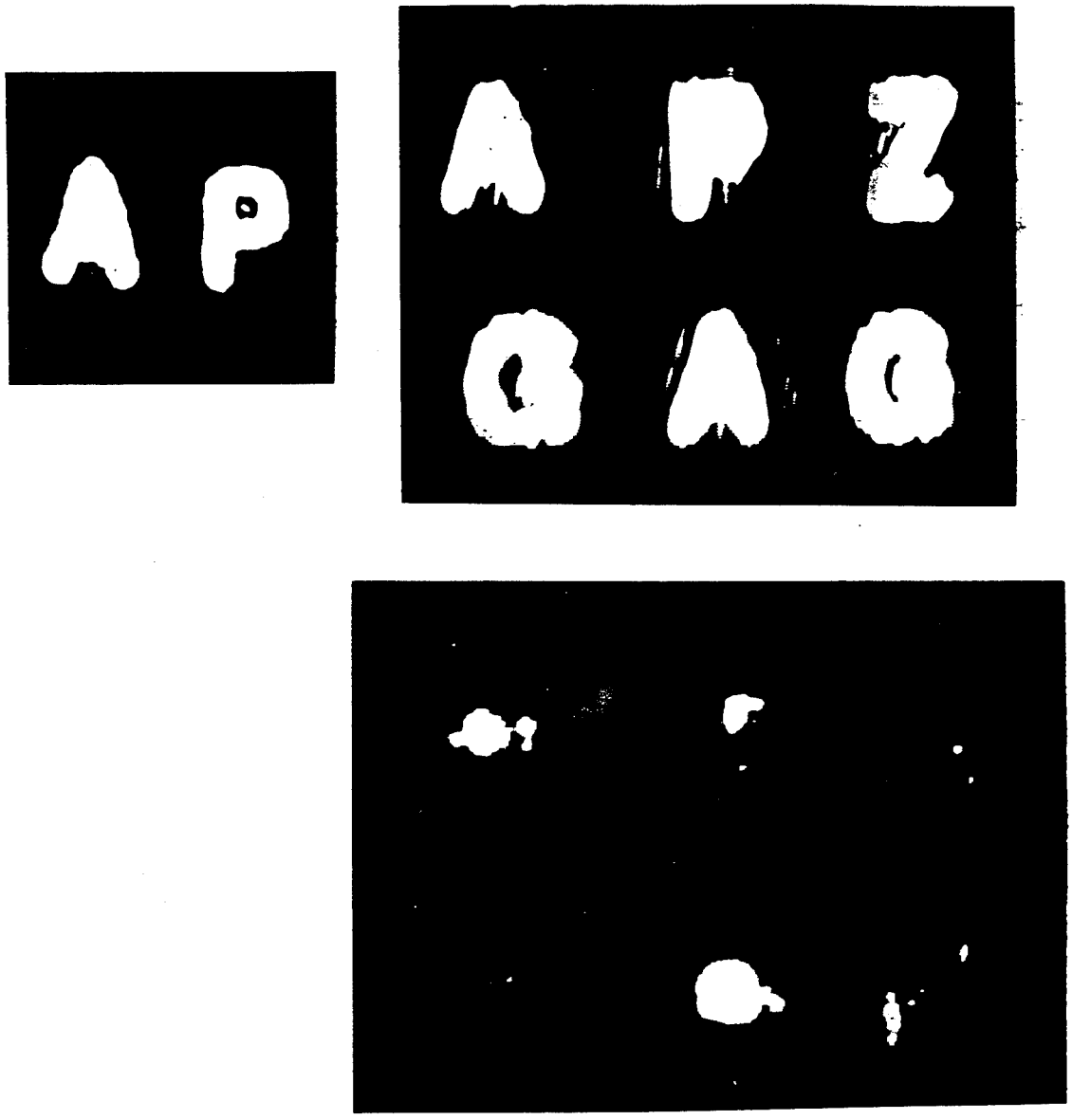

Figure 10: Pictures taken from the CCD TV monitor demonstrating pattern recognition using a chemically enhanced bR film in the Fourier plane. In this experiment, the input image was composed of two letters A and P. They were cross correlated with the six letter library pattern containing the letters A, P, Z, G, A, and G. The corresponding pattern recognition signals are shown in the bottom picture.

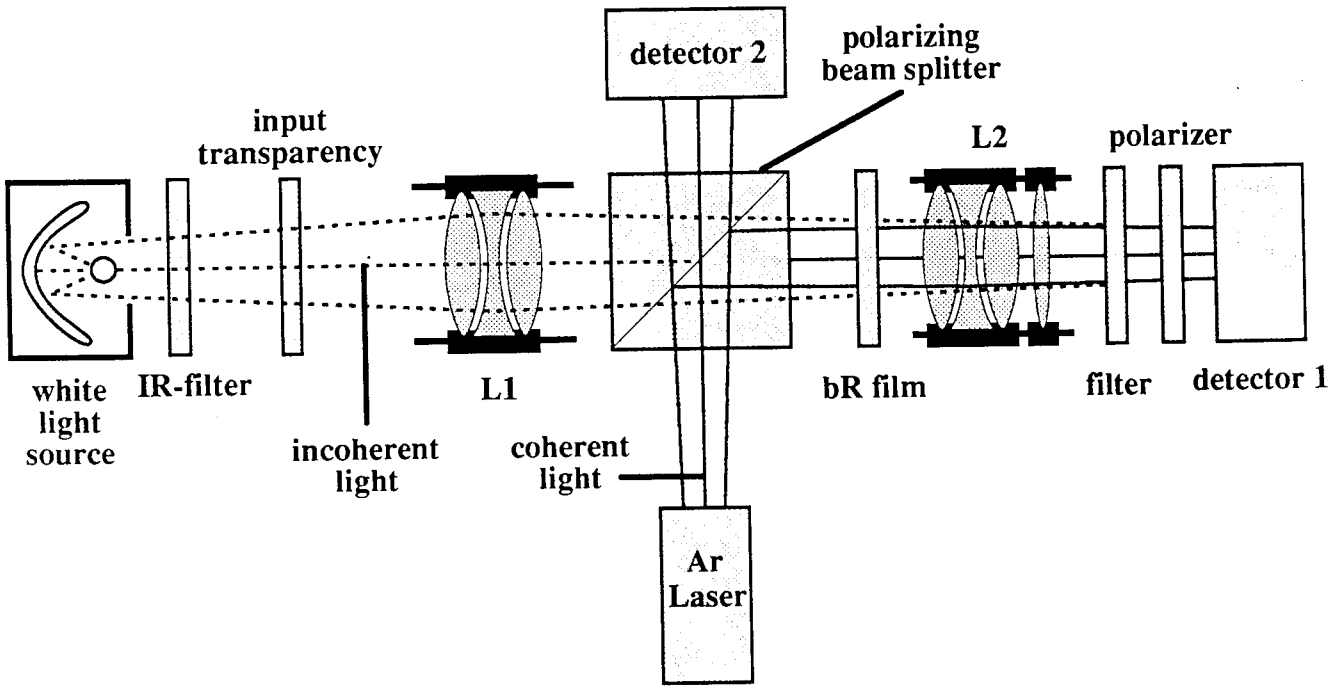

Figure 11: The experimental setup used for characterizing the transmission properties of an optically addressed spatial light modulator based on a thin film of bacteriorhodopsin. An input transparency, illuminated by a tungsten white light source, is imaged onto the BR film by lens L1. A bandpass filter (400 nm - 800 nm) selects only the visible portion of the spectrum emitted from the lamp. The 514 nm line from an Argon ion laser serves as the source of coherent readout. A narrow-band interference filter placed after the film eliminates transmitted white light from reaching the detector. The combination of a polarizing beam splitter and polarizer further excludes extraneous white light within the bandwidth of the interference filter such that only coherent laser light is detected at the output plane. Detectors 1 and 2 are used to monitor the intensities of the reading and writing light, respectively. For the experiment, the intensity of the readout beam was maintained at 0.16 mW/cm^2. The low intensity of the readout beam enabled non-destructive coherent readout of the image. Figure 12 shows the film's transmission response as a function of white light intensity for a 5x5 mm^2 input aperture.

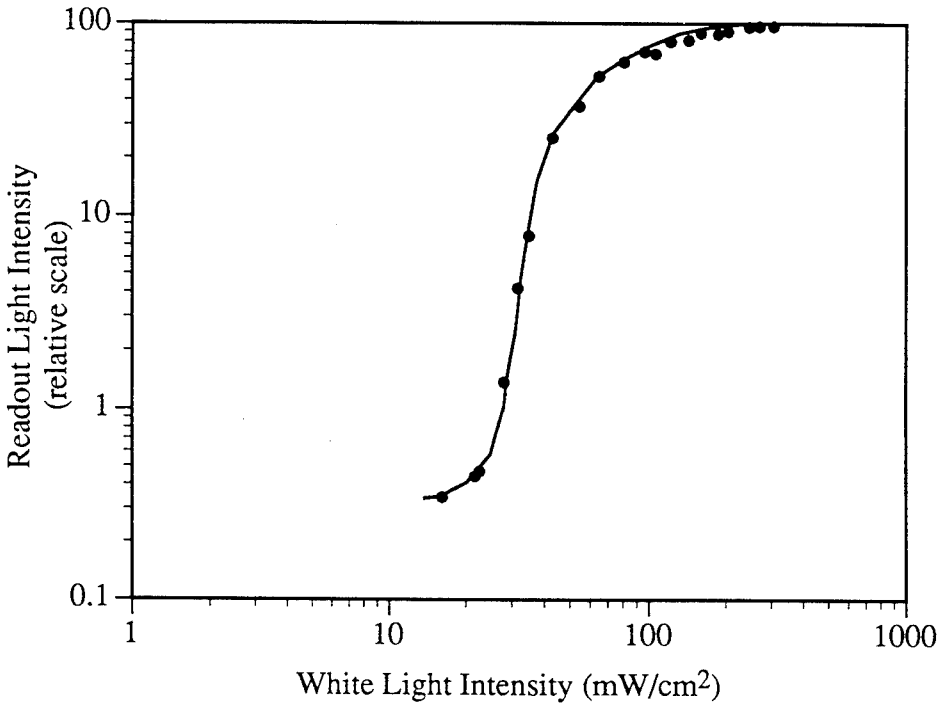

Figure 12: The relative transmission of a weak coherent readout beam (514 nm) as a function of incoherent white light intensity measured from the BR-SLM. The intensity of the readout beam was .16 mW/cm^2. The linear dynamic range of the device, which we define as the ratio of the maximum transmittance to the minimum transmittance, was calculated to be greater than 120. This value can be increased to greater than 10^3 by using the 570 nm line (krypton ion laser) as the readout wavelength.

Figure 13: A photograph of the reduced (.4X) resolution chart taken after readout from the BR-SLM: (left) the entire resolution chart; (right) an enlarged central portion of chart . The resolution of the film was found to be >100 line pairs/mm (group 5, element 3) after correction for demagnification, and was limited only by the resolution of the imaging optics.

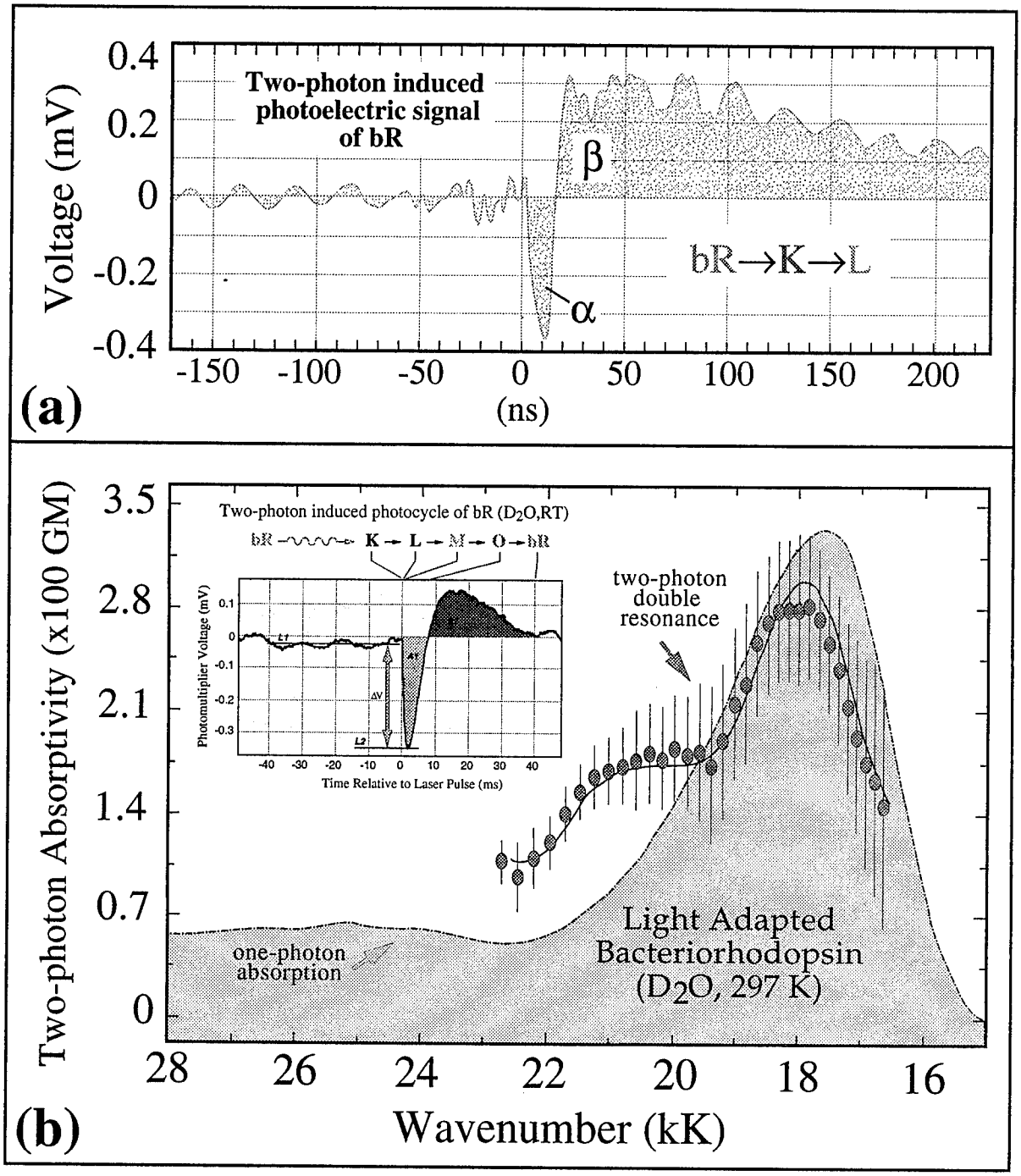

Figure 14. Dispersion of the two-photon absorptivity and the two-photon induced photoelectric signal of bacteriorhodopsin. The photoelectric signal for the oriented protein in polyacrylamide is shown in (a). The photoelectric signal is identical under one-photon versus two-photon excitation, and consists of two components, a fast component that follows the laser pulse and an oppositely polarized component that has a temporal profile that is pH and impedance dependant. Comparison of the one-photon absorption and the two-photon double resonance spectra of light-adapted bacteriorhodopsin is shown in (b). The insert to (b) shows the double resonance signal due to the absorption of the 633nm HeNe laser probe beam associated with the two-photon induced photocycle.

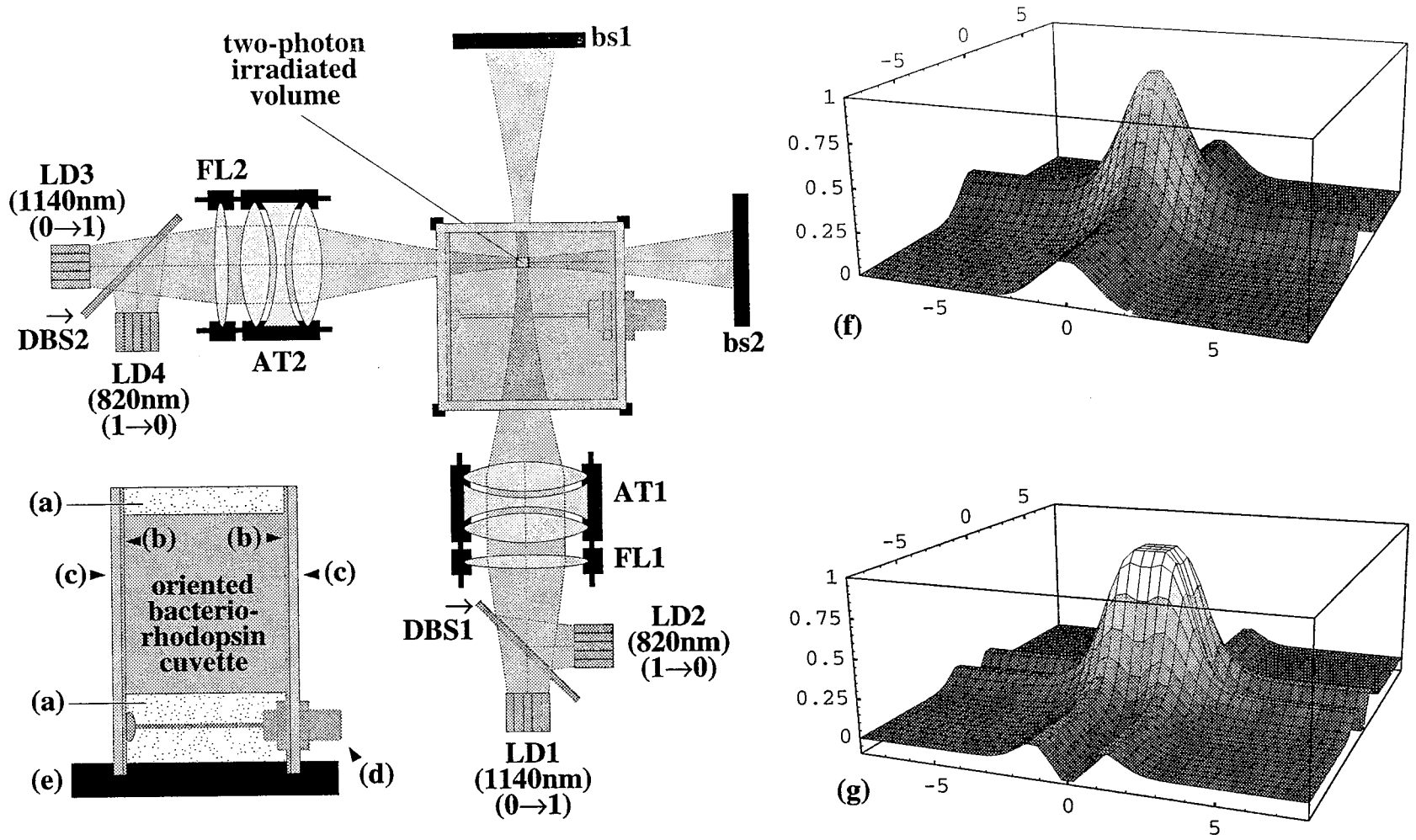

Figure 15. Schematic diagram of the principal optical components of a two-photon three-dimensional optical memory based on bacteriorhodopsin. The write operation involves the simultaneous activation of LD1 and LD3 (0→1) or LD2 and LD4 (1→0) to induce two-photon absorption within the irradiated volume and partially convert either **bR** to **M** (0→1) or **M** to **bR** (1→0). The write operation uses a 10 ns pulse and a pulse simultaneity of 1 ns. The protein is oriented within the cuvette by using an electric field prior to polymerization of the polyacrylamide gel. A polymer sealant is then used to maintain the correct polymer humidity. The SMA connector is attached to the indium-tin-oxide conducting surfaces on opposing sides of the cuvette and is used to transfer the photoelectric signal to the external amplifiers and box-car integrators. Symbols and letter codes are as follows: (a) sealing polymer, (b) indium-tin-oxide conductive coating, (c) BK7 optical glass; (d) SMA or OS50 connector; (e) Peltier temperature controlled base plate (0 - 20°C); AT (achromatic focusing triplet); bs (beam stop); DBS (dichroic beam splitter); LD (laser diode); FL (adjustable focusing lens). Computer simulations of the probability of two-photon induced photochemistry (vertical axis) as a function of location relative to the center of the irradiated volume (ΔX_{focus} and ΔY_{focus}) in microns are shown in (f) and (g). The upper right contour plot (f) shows the probability after two 1140 nm laser beams have been simultaneously directed along orthogonal axes crossing at the center of the irradiated volume. The lower right contour plot (g) shows the probability after two 820nm "cleaning pulses" have been independently directed along the same axes. The maximum conversion probability at x=0,y=0 is normalized to unity for both contour plots.

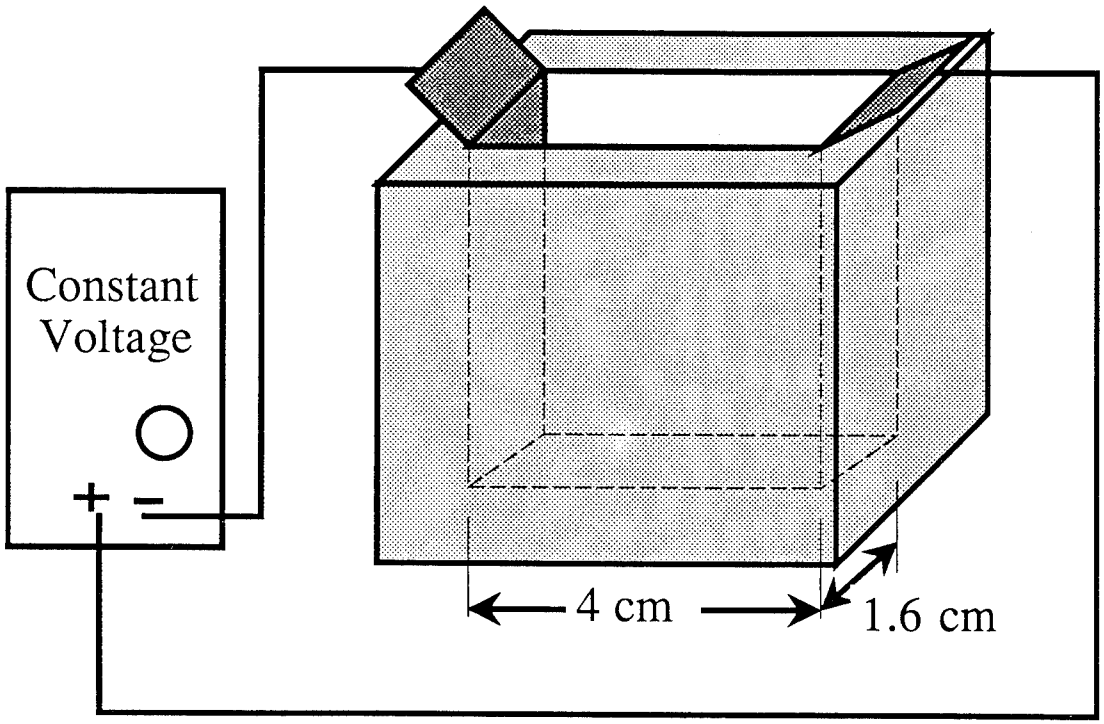

Figure 16. Experimental apparatus used to make oriented bR cubes for two-photon three-dimensional memory. The electrophoresis chamber is made of Telflon. The stainless steel electrodes in the chamber are 4 cm apart.

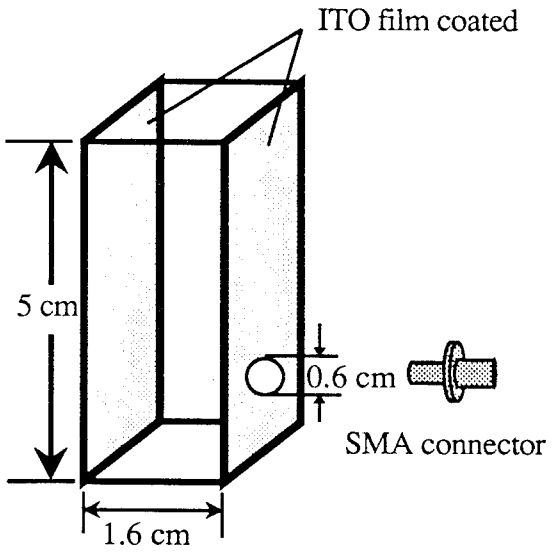

Figure 17. Photoelectrical gel holder for two-photon three-dimensional memory. The holder is made of glass plates with two of the pieces coated with ITO. The holder is assembled with epoxy. A small hole is drilled on one face of the holder to mount a SMA connector for the signal output.

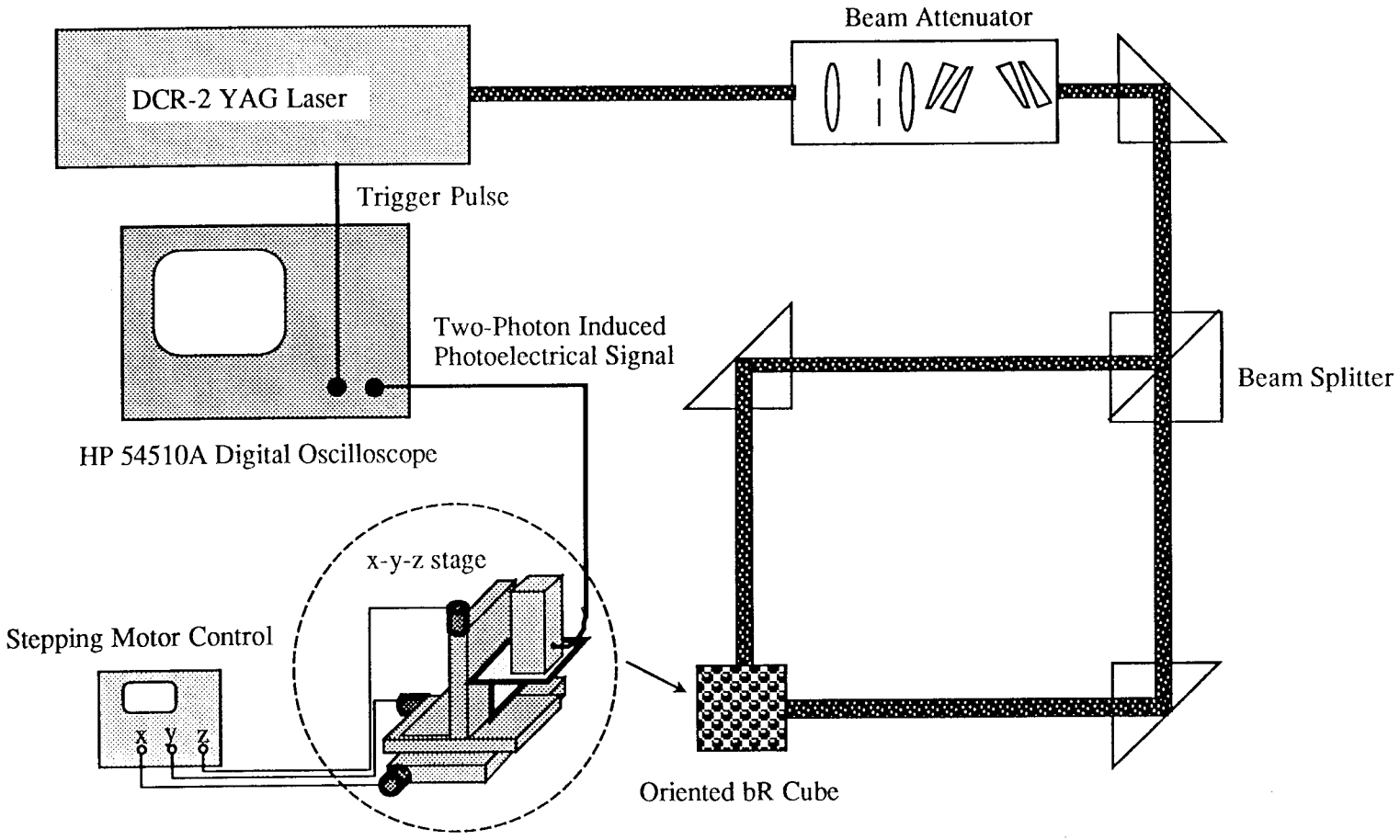

Figure 18. Experimental set-up for the characterization of two-photon three-dimensional memories. A 1.06 μm beam of a Q-switched YAG laser is used as the light source (DCR-2 from Spectra Physics). A beam attenuator (specially designed and constructed by Newport) is used to modulate the laser light intensity without shifting the beam position. The bR cube is mounted on a precision x-y-z stage which is controlled via stepping motors interfaced with a microprocessor (ATS 302 series from Areotech) . The photoelectrical signal is recorded with a 250 MHz bandwidth digital oscilloscope (HP54510A).

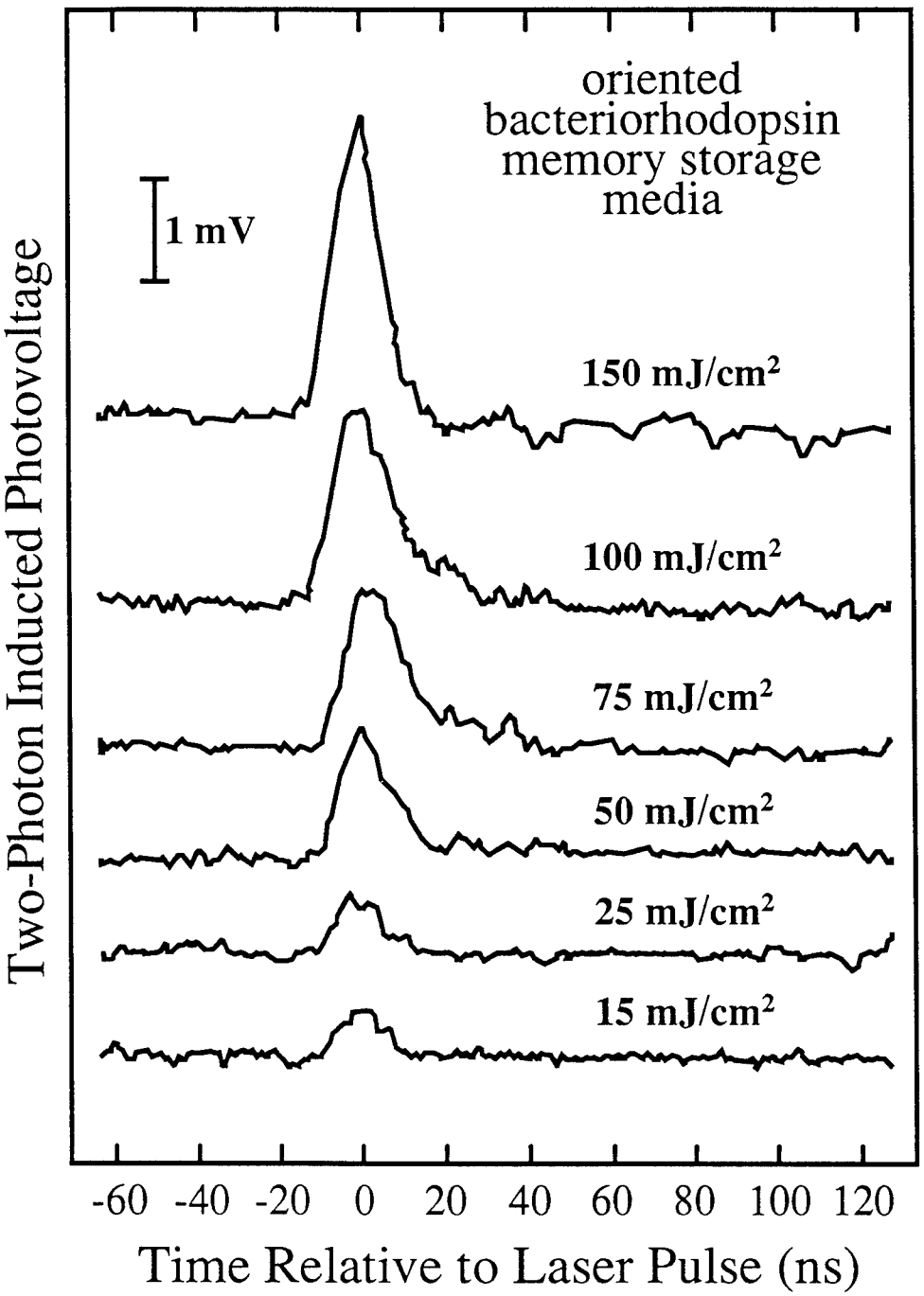

Figure 19. Measured photovoltages induced by two-photon absorption from an oriented bR cube for different laser energy densities. The excitation energy density of the 1.06 μm laser beam is indicated in each curve.

*U.S. GOVERNMENT PRINTING OFFICE: 1995-610-126-50140

MISSION

OF

ROME LABORATORY

Mission. The mission of Rome Laboratory is to advance the science and technologies of command, control, communications and intelligence and to transition them into systems to meet customer needs. To achieve this, Rome Lab:

a. Conducts vigorous research, development and test programs in all applicable technologies;

b. Transitions technology to current and future systems to improve operational capability, readiness, and supportability;

c. Provides a full range of technical support to Air Force Materiel Command product centers and other Air Force organizations;

d. Promotes transfer of technology to the private sector;

e. Maintains leading edge technological expertise in the areas of surveillance, communications, command and control, intelligence, reliability science, electro-magnetic technology, photonics, signal processing, and computational science.

The thrust areas of technical competence include: Surveillance, Communications, Command and Control, Intelligence, Signal Processing, Computer Science and Technology, Electromagnetic Technology, Photonics and Reliability Sciences.